Hindawi Publishing Corporation
Journal of Sensors
Volume 2008, Article ID 697062, 9 pages
doi:10.1155/2008/697062

Research Article

Characterizing Vibrating Cantilevers for Liquid Viscosity and Density Sensing

Christian Riesch,[1] Erwin K. Reichel,[2] Franz Keplinger,[1] and Bernhard Jakoby[2]

[1] *Institute of Sensor and Actuator Systems, Vienna University of Technology, Gusshausstrasse 27-29/366, 1040 Vienna, Austria*
[2] *Institute for Microelectronics and Microsensors, Johannes Kepler University, Altenberger Strasse 69, 4040 Linz, Austria*

Correspondence should be addressed to Christian Riesch, christian.riesch@tuwien.ac.at

Received 30 May 2008; Accepted 14 August 2008

Recommended by Maria Tenje

Miniaturized liquid sensors are essential devices in online process or condition monitoring. In case of viscosity and density sensing, microacoustic sensors such as quartz crystal resonators or SAW devices have proved particularly useful. However, these devices basically measure a thin-film viscosity, which is often not comparable to the macroscopic parameters probed by conventional viscometers. Miniaturized cantilever-based devices are interesting alternatives for such applications, but here the interaction between the liquid and the oscillating beam is more involved. In our contribution, we describe a measurement setup, which allows the investigation of this interaction for different beam cross-sections. We present an analytical model based on an approximation of the immersed cantilever as an oscillating sphere comprising the effective mass and the intrinsic damping of the cantilever and additional mass and damping due to the liquid loading. The model parameters are obtained from measurements with well-known sample liquids by a curve fitting procedure. Finally, we present the measurement of viscosity and density of an unknown sample liquid, demonstrating the feasibility of the model.

1. INTRODUCTION

For many applications like online process or condition monitoring, the liquid parameters viscosity and mass density are of high relevance. The use of conventional laboratory equipment is often not applicable due to its cost, space requirements, and other preconditions, for example, vibration-free mounting. Furthermore, sample taking for such devices often involves manual labor, tending to be time consuming and error-prone.

Microacoustic sensors like quartz thickness shear mode (TSM) resonators [1, 2] and surface acoustic wave (SAW) devices, for example, [3] have proved particularly useful alternatives to traditional viscometers [4]. However, these devices measure viscosity at comparatively high-shear rates and small vibration amplitudes. For non-Newtonian liquids, the results are, therefore, not directly comparable to those obtained from conventional viscometers. For complex liquids such as emulsions, it has also been shown that microacoustic devices may not be sufficient to detect rheological effects which are present only on the macroscopic scale [5].

Micromachined vibrating structures usually feature lower resonance frequencies and higher vibration amplitudes, making them more suitable for non-Newtonian and complex liquids [6]. Microcantilevers commonly used in atomic force microscopy [7–9] have been successfully used as liquid property sensors. They allow for simultaneous measurement of the liquid's viscosity and mass density, requiring sample volumes of less than 1 nL [10]. However, a highly sensitive optical readout is required to determine the beam's vibration amplitudes. When immersed in liquid, the cantilevers face strong deterioration of the quality factor due to high-dissipative effects [10]. Consequently, the vibration amplitudes drops even more, limiting the sensor's measurement range to low-viscous liquids. In other works, micromachined cantilevers and doubly clamped beams driven by Lorentz forces [6, 11–13] or by the piezoelectric effect [14, 15] have been utilized as liquid property sensors, and the feasibility of these sensors has been demonstrated for viscosities in the range up to several Pa·s.

In this contribution, we characterize resonating cantilevers for the measurement of mass density and viscosity

of liquids. They measure viscosity in a rheological domain which is more comparable to that probed by conventional laboratory instruments. The cantilevers feature piezoelectric excitation as well as piezoelectric readout. The vibrating part is about 55 mm long, but since only the cantilever tip is immersed in the liquid, the induced damping of the cantilever vibration is kept low. The sensors, therefore, exhibit high-quality factors, ranging from 20 to 60 even for highly viscous liquids. Consequently, the detection of the resonances could be accomplished by a simple readout electronics, and the measurement range is greatly extended. On the other hand, the sensitivity of the sensor is decreased. Furthermore, the sensor principle allows attaching different tips of well-defined geometries to the cantilevers.

When the cantilever tip is immersed in a liquid, the resonance frequency and the damping of the cantilever are influenced by the viscosity and density of the liquid. However, the cantilevers do not show a simple relationship between the result of such a measurement and the liquid parameters. Recently, several models have been devised to give a proper description of the interaction of a vibrating cantilever and the surrounding liquid, for example, [16–18] but most of these models assume fully immersed cantilevers, which are long and thin, that is, the width w is much smaller than the length L. For the designs considered in this work, only the cantilever tip is immersed in the liquid. For modeling the sensor-fluid interaction, the cantilever length L must therefore be replaced by the dipping depth d, which is in the same range as w. A solution for cantilevers featuring $w \approx L$, and accordingly $w \approx d$ is given in [19]. In [14] and other works, the influence of the liquid loading on the cantilever's frequency characteristics has been successfully modeled by approximating the forces acting on the cantilever tip by those acting on a sphere oscillating in a fluid. The results indicate that the cantilever tip is subject to an additional mass loading and an additional damping caused by the surrounding liquid.

In our work, we present a vibrating cantilever sensor and a setup for the measurement of viscosity and density. The interaction of the sensor and the liquid in which the tip is immersed is modeled by an oscillating sphere. Possible simplifications of the model are discussed, and a general model is devised. This model allows for simple calibration of the sensor in a set of liquids with well-known properties. Therefore, the knowledge of mechanical and electrical properties of the cantilever is not required, the model parameters are instead obtained from the calibration procedure.

2. SENSOR FABRICATION

The cantilever sensors used in this work are based on commercially available lead zirconate titanate (PZT) bimorph bending actuators (Argillon GmbH, Redwitz, Germany). They feature a length of 49.95 mm, a width of 7.2 mm, and a total thickness of 0.8 mm [20]. The cantilevers consist of two piezoelectric PZT layers on both sides of a carbon fiber substrate (Figure 1(a)). The PZT layers are polarized in thickness direction. Electrodes (1, 2, 3) allow for excitation

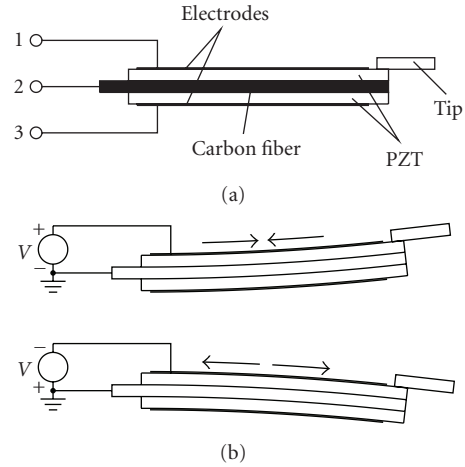

Figure 1: (a) PZT bending actuator with attached tip. The bending actuator consists of a carbon fiber substrate and two piezoelectric layers. The electrodes (1, 2, 3) allow for excitation and readout of the sensor. (b) Applying a voltage to the upper layer leads to contraction or elongation of the upper layer as indicated by the arrows.

Table 1: Tip geometries (rectangular cross-section) and tip materials.

Tip	Width w	Thickness	Material
Tip A	7 mm	0.5 mm	silicon
Tip B	5 mm	0.5 mm	silicon
Tip C	4 mm	0.3 mm	brass
Tip D	2 mm	0.5 mm	silicon

of the actuator. Applying a voltage between the top electrode (electrode 1) and the center electrode (2 in Figure 1(a)), which is used as ground electrode (Figure 1(b)) causes a contraction or elongation in the upper PZT layer but not in the substrate, and, therefore, deforms the cantilever. In our setup (Figure 2(a)) a sinusoidal voltage is applied, which leads to bending vibrations of the beam. A maximum voltage of 200 V can be applied to the cantilever. The actual beam deflection is determined by measuring the voltage at the sensing electrode.

The bending actuator is clamped at one end, whereas different tips of well-defined cross-sections are attached to the free end. These tips are immersed in the sample liquid. The tip geometries and materials are given in Table 1. The clamping fixture is mounted on a rigid frame allowing for vertical (x-direction) positioning of the sensor and preventing vibrations of the entire setup. A lock-in amplifier (LIA) measures the sensor voltage V_s, resulting in the cantilever's frequency response. As voltage source V_d, the internal oscillator of the lock-in amplifier is used.

The cantilever exhibits several resonant vibration modes. As an example, Figure 3(a) shows the deflection (z-direction) for a cantilever with tip A (Table 1) vibrating in air. The corresponding sensing electrode voltage is shown in the diagram below (Figure 3(b)). The resonance frequencies are 100 Hz and 851 Hz for the first and second modes, respectively. Further resonances were found at 2456 Hz

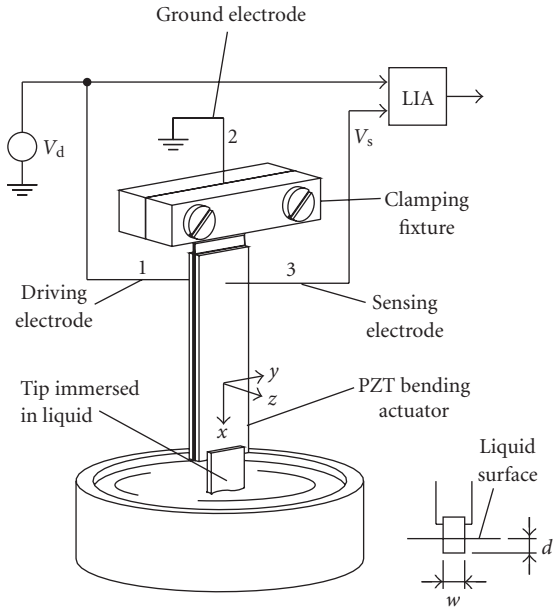

Figure 2: Measurement setup. The PZT bending actuator is rigidly clamped at one end. To the free end of the cantilever, a tip of well-defined geometry (width w) is attached and immersed in the sample liquid (dipping depth d). The interaction of the cantilever tip and the liquid changes the frequency characteristics, which is measured by the lock-in amplifier (LIA).

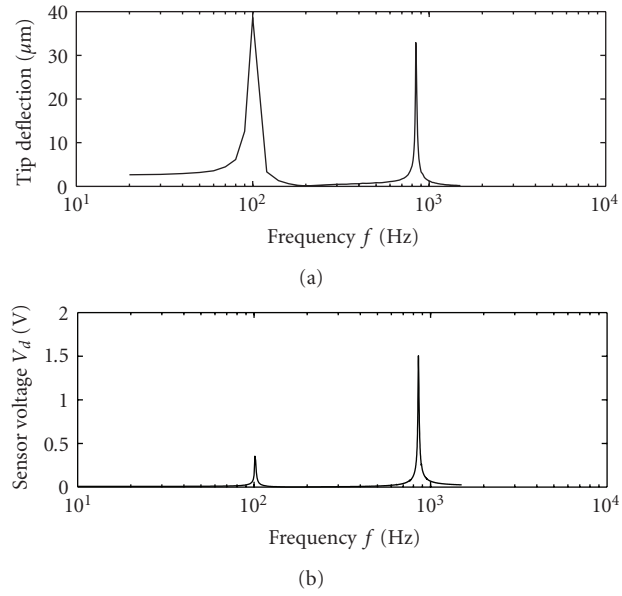

Figure 3: Frequency characteristics of a PZT cantilever with tip A (Table 1), $V_d = 400\,mV_{rms}$ driving voltage, vibrating in air. (a) The tip deflection (peak-peak) was measured using a Polytec OFV-5000/OFV-505 laser vibrometer. (b) The diagram below shows the corresponding sensing electrode rms voltage.

(3rd mode) and 4870 Hz (4th mode). The mode shapes for a uniform cantilevered beam without a load at the tip are given in Figure 4 [21].

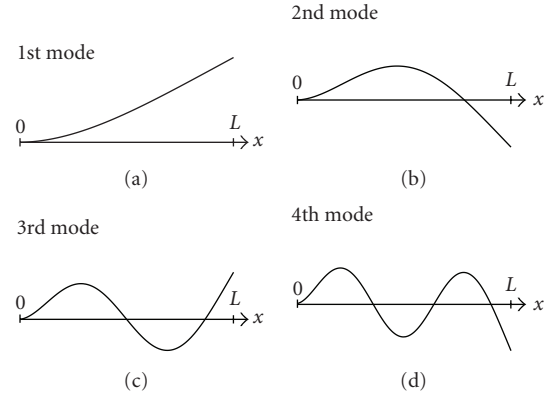

Figure 4: Mode shapes of a uniform cantilevered beam. The mode shapes have been obtained from solutions of the Euler-Bernoulli beam equation and are also roughly valid for the piezoelectric bimorph.

3. THEORETICAL MODEL

The vibration behavior of the piezoelectric bending actuator is described by the Euler-Bernoulli beam equation [21]:

$$EI\frac{\partial^4\psi(x,t)}{\partial x^4}+\mu\frac{\partial^2\psi(x,t)}{\partial t^2}=\frac{\partial^2 M_p(x,t)}{\partial x^2}, \tag{1}$$

where EI and μ are the effective bending stiffness and the effective mass per unit length of the composite beam, $\psi(x,t)$ is the beam deflection in z-direction (Figure 2), and M_p is the actuating moment due to the piezoelectric effect. Since M_p is considered to be a constant moment along the entire beam, $\partial^2 M_p/\partial x^2 = 0$. Consequently, the boundary conditions for the clamped-free beam are

$$\begin{aligned}\psi(0,t)&=0,\\ \frac{\partial\psi(0,t)}{\partial x}&=0,\\ \frac{\partial^2\psi(L,t)}{\partial x^2}&=\frac{1}{EI}M_p,\\ \frac{\partial^3\psi(L,t)}{\partial x^3}&=-\frac{1}{EI}F,\end{aligned} \tag{2}$$

where L is the length of the beam and F is the force acting on the tip due to the interaction with the surrounding liquid. The actuating moment M_p is given by [22]

$$M_p=\int_{A_p} Y_p d_{31} E_z z\,dA = w_b Y_p d_{31} V_d z_m, \tag{3}$$

where A_p, Y_p, and d_{31} are the cross-sectional area, Young's modulus, and the piezoelectric modulus of the actuating layer and E_z is the electric field in this layer in z-direction. w_b is the width of the bending actuator, z_m is the mean distance of the actuating layer from the beam center, and V_d is the excitation voltage (Figure 2(a)).

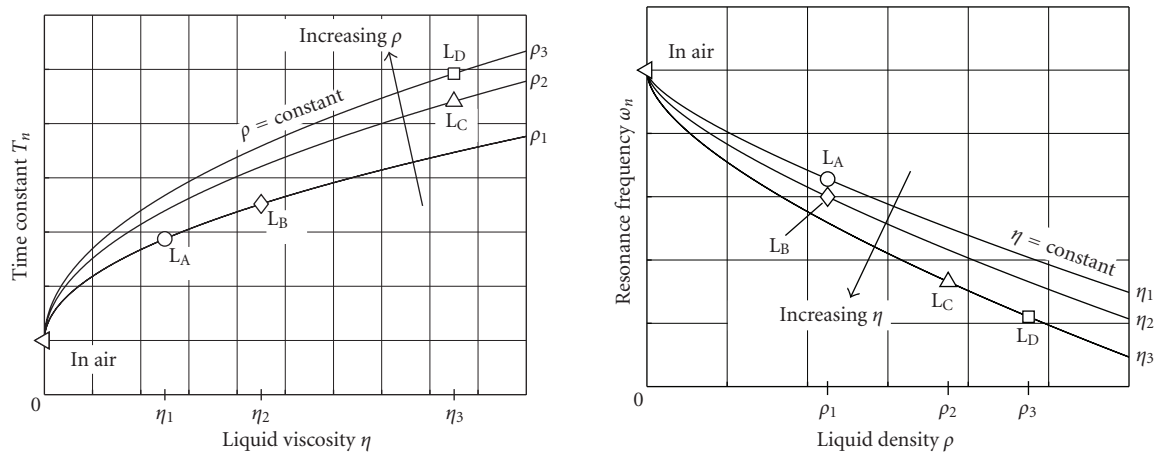

FIGURE 5: Time constant T_n and resonance frequency ω_n of a resonant cantilever dipping in 4 different sample liquids L_A, L_B, L_C, and L_D as given by the generalized models (15) and (16).

The measured voltage V_s is calculated by applying

$$D_z = d_{31} T_{xx} + \varepsilon E_z,$$
$$T_{xx} = \frac{1}{K_{11}} (S_{xx} - d_{31} E_z) \tag{4}$$

to the sensing PZT layer, where D_z, T_{xx}, and S_{xx} are electric displacement, stress, and strain. ε and K_{11} are the permittivity and the compliance of the PZT layer. Since V_s is measured by means of a voltage amplifier in our setup, the current I_s from the sensing electrode vanishes, and, therefore, the charge:

$$Q = \int_{A_e} D_z \mathrm{d}A = 0, \tag{5}$$

where A_e is the surface area of the sensing electrode. From (4), (5), and $S_{xx} = -z\partial^2\psi(x,t)/\partial x^2$,

$$V_s(t) = K_v \frac{\partial \psi(L,t)}{\partial x} \tag{6}$$

is obtained, where K_v is a constant depending on material and geometry parameters [22]. The voltage at the sensing electrode is given by the slope of the beam deflection $\psi(x,t)$ at the free end, $x = L$, of the cantilever. This fact is greatly confirmed by the measurements given by Figure 3. Despite the lower tip deflection amplitude of the second mode the resulting output voltage is higher than for the first mode of vibration.

The interaction with the liquid surrounding, the cantilever tip can be modeled by approximating the vibrating cantilever as an oscillating sphere immersed in a liquid [14], exhibiting an effective sphere radius R and an effective sphere mass. The force F acting on such a sphere is given by [23]

$$F = 6\pi\eta R\left(1 + \frac{R}{\delta}\right)\frac{\mathrm{d}u}{\mathrm{d}t} + 3\pi R^2\sqrt{\frac{2\eta\rho}{\omega}}\left(1 - \frac{2R}{9\delta}\right)\frac{\mathrm{d}^2u}{\mathrm{d}t^2}, \tag{7}$$

where u is the sphere displacement, R is the sphere radius, ω is the angular oscillation frequency, and δ is the depth of penetration of the acoustic wave, which is given by

$$\delta = \sqrt{\frac{2\eta}{\omega\rho}}. \tag{8}$$

The tips are attached to the free ends of the cantilevers, therefore, the sphere displacement is $u = \psi(L,t)$.

In principle, solving the equations given above yields the frequency characteristics of the vibrating cantilever with a tip immersed in liquid for all modes of vibration. As the cantilever represents a composite structure involving layers featuring different material properties, effective parameters have to be used in the beam equation, for example, for Young's modulus. As also the material parameters of the layers are not, or only partly, available in the required accuracy and since the solution of the beam equation would require the solution of a higher order system in order to determine the coefficients by a suitable expansion (e.g., eigenmode expansion), we have approximated the resonance behavior of the sensor in the vicinity of the first mode resonance frequency as a second-order system, given by

$$(M_e + M_i)\frac{\mathrm{d}^2u}{\mathrm{d}t^2} + (b_e + b_i)\frac{\mathrm{d}u}{\mathrm{d}t} + Ku = F_0 e^{\mathrm{j}\omega t}, \tag{9}$$

where u is the deflection of the cantilever tip in z-direction (Figure 2), M_e and b_e are the effective mass and the intrinsic damping of the cantilever and the tip, K is the spring constant, and F_0 and ω are the driving force amplitude and angular frequency. M_i and b_i are the induced mass and damping due to the liquid loading, given by (7)

$$M_i = 3\pi R^2\sqrt{\frac{2\eta\rho}{\omega}}\left(1 - \frac{2R}{9\delta}\right), \tag{10}$$

$$b_i = 6\pi\eta R\left(1 + \frac{R}{\delta}\right). \tag{11}$$

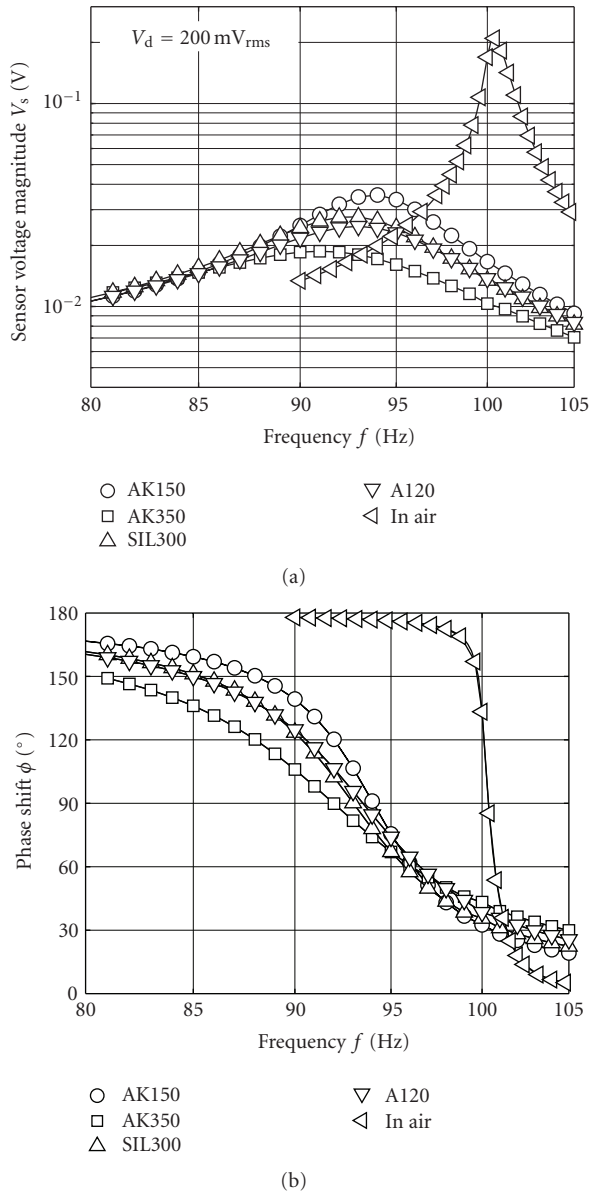

Figure 6: Magnitude and phase response of a cantilever with tip A vibrating in air and immersed in different liquids (Table 2). The dipping depth d is 2 mm, the driving voltage $V_d = 200\,mV_{rms}$.

For sample liquids exhibiting high viscosities, and low-vibration frequencies, R is negligible compared to δ, leading to a simplification of (10) and (11) [14]. For the considered cantilever tips and dipping depths (Table 1), the effective sphere radius R is in the range of a few millimeters. The expected penetration depths δ for the sample liquids used in this work were calculated for a vibration frequency of 100 Hz and are given in Table 2. The results show that δ is in the same range as R, and the prerequisites for said simplification are not fulfilled.

Consequently, the consideration of the characteristic penetration depth δ leads to a frequency dependence of the liquid mass loading M_i, (cf. (10)), and the liquid damping b_i (cf. (11)). In the following, both M_i and b_i are considered constant in the vicinity of the resonance frequency, which is justified by the high-quality factors and the accompanied narrow bandwidths of the resonances. Therefore, solving the differential equation (9) using the Laplace transform yields

$$U(s) = \frac{1}{1 + (2D_n/\omega_n)s + (1/\omega_n^2)s^2} F(s), \tag{12}$$

where $U(s)$ and $F(s)$ are the Laplace transforms of the tip deflection u and the driving force:

$$\begin{aligned} \frac{1}{\omega_n^2} &= \frac{M_e + M_i}{K}, \\ \frac{2D_n}{\omega_n} &= \frac{b_e + b_i}{K}, \end{aligned} \tag{13}$$

where ω_n is the resonance frequency and D_n the damping factor of the respective vibration mode. From (7) and (13), one obtains

$$\begin{aligned} \omega_n^2 &= \omega_{n,\mathrm{air}}^2 \frac{1}{1 + (2\pi R^3/3M_e)\rho + (6\pi R^2/\sqrt{2}M_e)(1/\sqrt{\omega_n})\sqrt{\eta\rho}}, \\ \frac{2D_n}{\omega_n} &= \frac{2D_{n,\mathrm{air}}}{\omega_{n,\mathrm{air}}} \left(1 + \frac{6\pi R}{b_e}\eta + \frac{6\pi R^2}{\sqrt{2}b_e}\sqrt{\omega_n}\sqrt{\eta\rho}\right), \end{aligned} \tag{14}$$

where $\omega_{n,\mathrm{air}}$ and $D_{n,\mathrm{air}}$ are the resonance frequency and damping factor of the cantilever without liquid loading. The oscillating sphere model shows that the cantilever's resonance frequency is affected by a term related to the liquid density, and a second term containing the viscosity-density product, whereas the time constant $T_n = 2D_n/\omega_n$ depends on the viscosity and the viscosity-density product.

For the interpretation of our measurement results involving rectangular cross-sections, we devised a more generalized model. Based on (14) and by introducing four independent coefficients c_1, c_2, c_3, and c_4, we have

$$\omega_n^2 = \omega_{n,\mathrm{air}}^2 \frac{1}{1 + c_1\rho + c_2(1/\sqrt{\omega_n})\sqrt{\eta\rho}}, \tag{15}$$

$$T_n = T_{n,\mathrm{air}}(1 + c_3\eta + c_4\sqrt{\omega_n}\sqrt{\eta\rho}), \tag{16}$$

where $T_{n,\mathrm{air}}$ is the in-air time constant $2D_{n,\mathrm{air}}/\omega_{n,\mathrm{air}}$. The values of the parameters c_i are determined by the tip size and geometry, the effective cantilever mass and damping, the dipping depth d (Figure 2(b)), and the respective mode of vibration n.

Figure 5 elucidates the model given by (15) and (16). We consider four liquids L_A, L_B, L_C, and L_D of which L_A and L_B are of the same density ρ_1, whereas L_C and L_D are of the same viscosity η_3. The expected values of ω_n and T_n are given by markers in the figure. The curves in the figure represent the results expected for liquids of the same viscosity and density, respectively.

For the determination of viscosity and density of an unknown liquid, (15) and (16) have to be solved for η and ρ. The system of equations can be written as

$$\begin{aligned} A &= B\rho + C\sqrt{\eta\rho}, \\ D &= E\sqrt{\eta\rho} + F\eta, \end{aligned} \tag{17}$$

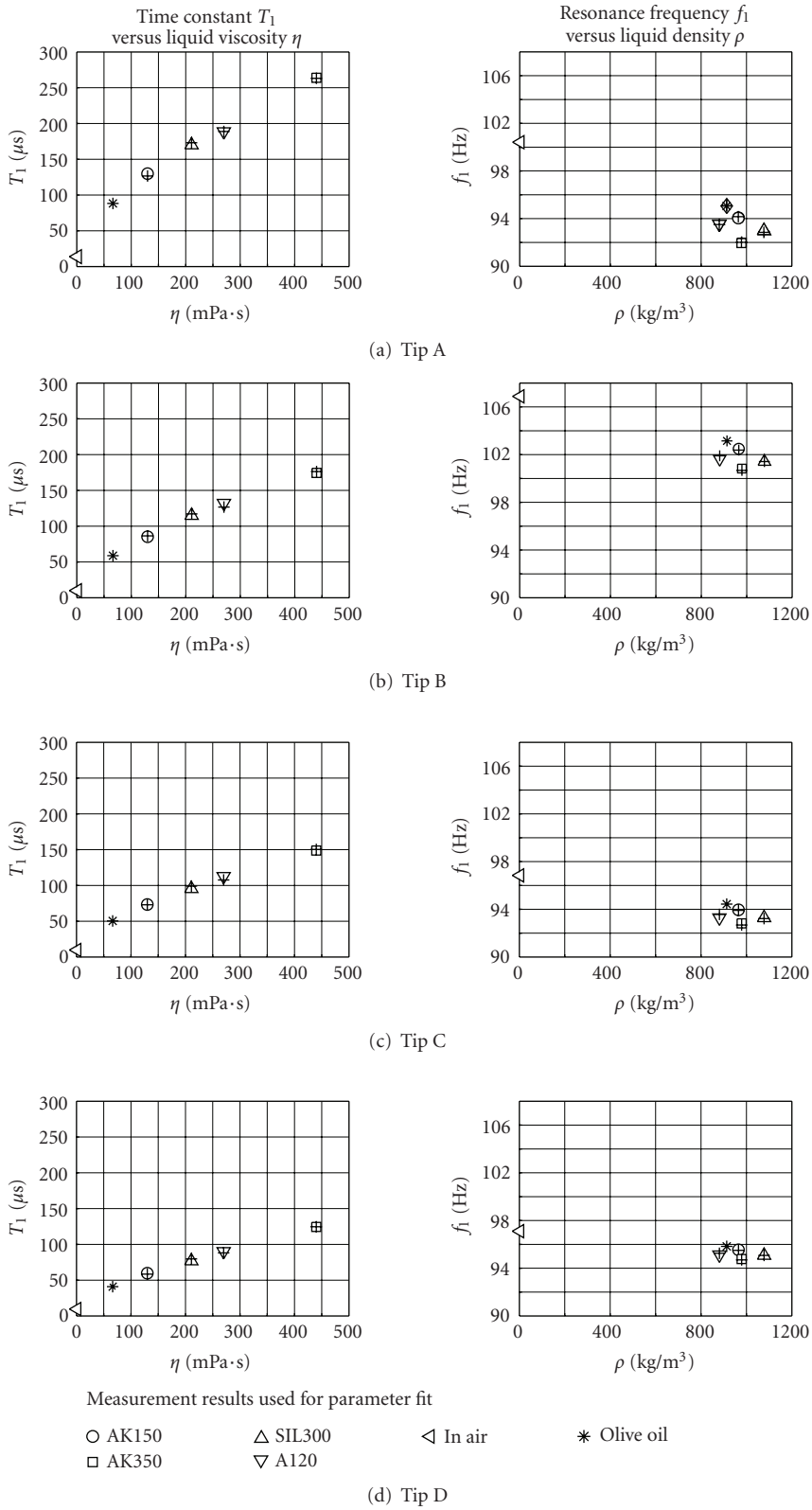

Figure 7: Resonance frequency ω_1 and time constant T_1 obtained for the four different tips and a variety of sample liquids. The crosses (+) in the diagrams represent the calculated values obtained from the parameter fit and show good agreement between the experimental results and the model.

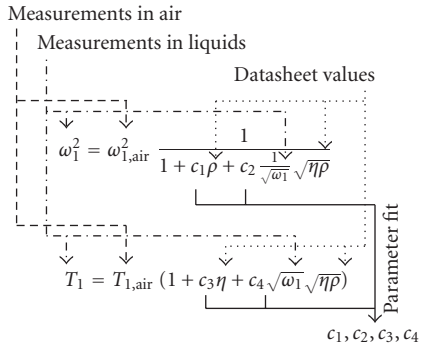

Figure 8: Obtaining the model parameters c_1, c_2, c_3, and c_4 from measurements (Figure 7) in air and in reference liquids with known viscosities and densities (Table 2).

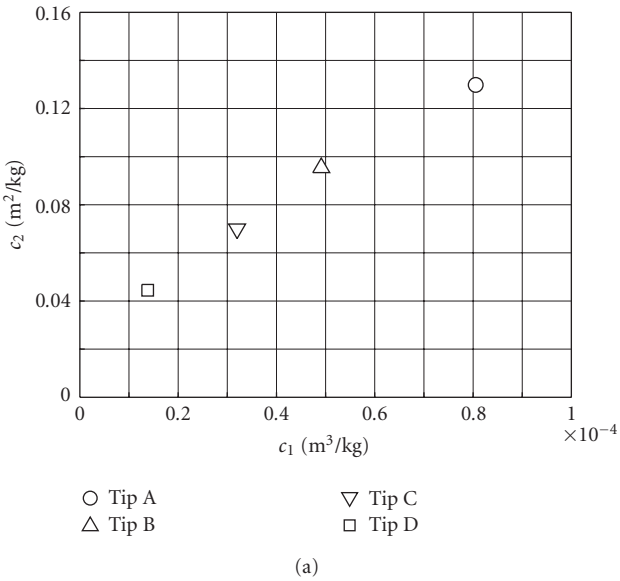

(a)

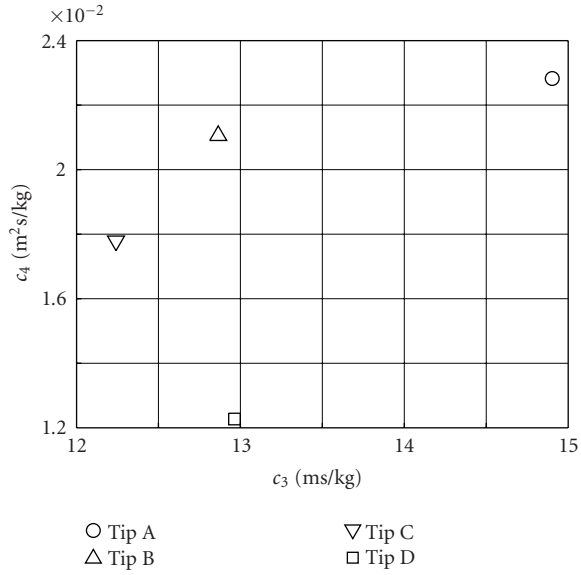

(b)

Figure 9: Fitted parameter values c_1, c_2, c_3, and c_4 obtained by fitting the model equations to the measurement results.

where $A = \omega_{n,\text{air}}^2/\omega_n^2 - 1$, $B = c_1$, $C = c_2/\sqrt{\omega_n}$, $D = T_n/T_{n,\text{air}} - 1$, $E = c_4\sqrt{\omega_n}$, and $F = c_3$. Solving the system of equations yields

$$\begin{aligned}
\rho_{1,2} &= -\frac{1}{2}\frac{ACE - 2ABF - C^2D}{B(BF - CE)} \\
&\quad \pm \sqrt{\frac{1}{4}\frac{(ACE - 2ABF - C^2D)^2}{B^2(BF - CE)^2} - \frac{A^2F}{B(BF - CE)}}, \\
\eta_{1,2} &= -\frac{1}{2}\frac{CDE - 2BDF - AE^2}{F(BF - CE)} \\
&\quad \pm \sqrt{\frac{1}{4}\frac{(CDE - 2BDF - AE^2)^2}{F^2(BF - CE)^2} - \frac{BD^2}{F(BF - CE)}}.
\end{aligned} \tag{18}$$

For the cantilevers used in this work, it turns out that $BF - CE = c_1c_3 - c_2c_4 < 0$. Furthermore, all the coefficients of (17) are positive, that is, $A, B, C, D, E, F > 0$. Therefore, in (18), only that $\rho_{1,2}$ and $\eta_{1,2}$, respectively, are positive which exhibit a plus before the root sign, that is,

$$\begin{aligned}
\rho &= -\frac{1}{2}\frac{(c_2c_4 - 2c_1c_3)\left(\frac{\omega_{n,\text{air}}^2}{\omega_n^2} - 1\right) - \frac{c_2^2}{\omega_n}\left(\frac{T_n}{T_{n,\text{air}}} - 1\right)}{c_1(c_1c_3 - c_2c_4)} \\
&\quad + \left\{\frac{1}{4}\frac{\left[(c_2c_4 - 2c_1c_3)\left(\frac{\omega_{n,\text{air}}^2}{\omega_n^2} - 1\right) - \frac{c_2^2}{\omega_n}\left(\frac{T_n}{T_{n,\text{air}}} - 1\right)\right]^2}{c_1^2(c_1c_3 - c_2c_4)^2}\right. \\
&\quad \left. - \frac{c_3\left(\frac{\omega_{n,\text{air}}^2}{\omega_n^2} - 1\right)^2}{c_1(c_1c_3 - c_2c_4)}\right\}^{1/2}, \\
\eta &= -\frac{1}{2}\frac{(c_2c_4 - 2c_1c_3)\left(\frac{T_n}{T_{n,\text{air}}} - 1\right) - c_4^2\omega_n\left(\frac{\omega_{n,\text{air}}^2}{\omega_n^2} - 1\right)}{c_3(c_1c_3 - c_2c_4)} \\
&\quad + \left\{\frac{1}{4}\frac{\left[(c_2c_4 - 2c_1c_3)\left(\frac{T_n}{T_{n,\text{air}}} - 1\right) - c_4^2\omega_n\left(\frac{\omega_{n,\text{air}}^2}{\omega_n^2} - 1\right)\right]^2}{c_3^2(c_1c_3 - c_2c_4)^2}\right. \\
&\quad \left. - \frac{c_1\left(\frac{T_n}{T_{n,\text{air}}} - 1\right)^2}{c_3(c_1c_3 - c_2c_4)}\right\}^{1/2}.
\end{aligned} \tag{19}$$

4. MEASUREMENTS

With the setup depicted in Figure 2(a), the frequency response of the cantilevers is examined. The lock-in amplifier (Stanford Research SR830) is used to drive the cantilever and to measure the sensor voltage V_s and the phase shift $\phi(j\omega)$ between the driving voltage, that is, the driving force and the sensor voltage, that is, the actual cantilever deflection.

Table 2: Reference values (dynamic viscosity η and mass density ρ) of the sample liquids used in the measurements and the expected depth of penetration δ at an angular frequency of $\omega = 2\pi \cdot 100\,\text{Hz}$, see (8). The dynamic viscosity was measured using a Brookfield LVDV+II-CP cone/plate rheometer at an ambient temperature of 23°C.

Sample liquid	Viscosity η	Density ρ	δ (100 Hz)
AK150 silicone oil	130 mPa·s	965 kg/m^3	0.65 mm
AK350 silicone oil	440 mPa·s	979 kg/m^3	1.2 mm
SIL300 silicone oil	211 mPa·s	1078 kg/m^3	0.79 mm
Alcatel A120 oil	270 mPa·s	881 kg/m^3	0.99 mm

Table 3: Determination of viscosity and density of an olive oil sample by means of vibrating cantilevers. The density ρ and the viscosity η have been calculated from the measurement results $\omega_1 = 2\pi f_1$ and T_1 using (19). The density and viscosity obtained by means of weighting and a cone-plate rotational viscometer, respectively, are $\eta_{\text{ref}} = 66.4\,\text{mPa}\cdot\text{s}$ and $\rho_{\text{ref}} = 913\,\text{kgm}^{-3}$.

Cantilever	f_1	T_1	Viscosity η	Density ρ
Tip A	95.07 Hz	88.24 μs	66.4 mPa·s	919.7 kgm^{-3}
Tip B	103.15 Hz	58.80 μs	62.9 mPa·s	921.4 kgm^{-3}
Tip C	94.44 Hz	50.43 μs	64.6 mPa·s	920.1 kgm^{-3}
Tip D	95.83 Hz	40.88 μs	67.6 mPa·s	908.6 kgm^{-3}

The measurements are carried out with a sinusoidal driving voltage of 200 mV_{rms} and within a frequency range from 70 to 110 Hz. At the resonance frequency of the first mode, a maximum tip deflection of 19 μm (peak-peak) was measured in air by means of a Polytec OFV-5000/OFV-505 laser vibrometer.

A variety of oils are used as test liquids: AK150, AK350 (Wacker Chemie), and SIL300 are silicone oils, and Alcatel 120 (A120) oil. They exhibit liquid densities in the range from 881 to 1078 kg/m^3 and viscosities from 145 to 440 mPa·s. These nominal liquid parameters are obtained from data sheets and measurements by means of a Brookfield LVDV+II-CP cone/plate rheometer (Table 2). The parameters of the liquids vary with temperature. As especially the viscosity is highly temperature dependent, temperature control of the liquid container has been established by means of a peltier heater/cooler system. All results presented here have been obtained at 23°C.

The dipping depth (Figure 2(b)) was adjusted by lowering the sensor until the tip touches the liquid surface, and then adding the desired $d = 2\,\text{mm}$, using a micrometer screw. For liquids exhibiting low-surface tensions, like those considered in this work, a concave meniscus is formed at the liquid-tip interface. We expect the resulting liquid surface shape to increase the effective dipping depth, and, therefore, to influence the sensor's behavior. Consequently, the sensor principle would be limited to liquids with similar surface tensions, which can be assumed for the considered oils.

Figure 6 summarizes the measurement results at mode 1 for tip A in air and immersed in the sample liquids. As expected from (15) and (16), the liquid loading decreases the resonance frequency ω_1 and increases the damping factor D_1.

From the cantilever's frequency response, we extract the first mode resonance frequency $\omega_1 = 2\pi f_1$ and the damping factor D_1 by fitting a second-order transfer function:

$$\phi(\text{j}\omega) = \arg\left\{\frac{1}{1 + \text{j}\omega(2D_1/\omega_1) - (\omega^2/\omega_1^2)}\right\} \tag{20}$$

to the phase shift measurements (Figure 6) with respect to the parameters ω_1 and D_1.

Figure 7 shows the results for the cantilevers with tips A, B, C, and D (Table 1) and the sample liquids (Table 2). The left column of Figure 7 shows the measured time constant $T_1 = 2D_1/\omega_1$ versus the dynamic viscosity η of the sample liquids. The results for each cantilever appear to be nearly lying on a single trend curve, indicating that T_1 is dominantly influenced by the liquid's dynamic viscosity. According to model equation (16), the value of c_4 thus must be small compared to c_3.

Figure 7, right column, depicts the resonance frequency f_1 versus the liquid density. The results are widely spread in the ρ-f_1 plane. Obviously, the resonance frequency of the cantilever tip immersed in the liquid is strongly influenced by both the liquid's density and viscosity. In our model, this relationship is described by (15).

Using the measurement results (Figure 7), the model parameters c_1, c_2, c_3, and c_4 can be determined. Figure 8 illustrates the model equations (15) and (16) and the parameter fit procedure. The values of $\omega_{1,\text{air}}$ and $T_{1,\text{air}}$ are obtained from a single measurement of the vibrating cantilever in air. Furthermore, each measurement in a sample liquid yields a pair of (ω_1, T_1). The values of viscosity and density, η and ρ, of each sample liquid are also known (Table 2). Finally, a fit algorithm applied to the model equations results in the model parameters c_1, c_2, c_3, and c_4 for a particular cantilever. The results of this parameter fit are depicted in Figure 9. The diagram shows the model parameters c_1, c_2, c_3, c_4 for the cantilevers with different tips. It is important to note that the parameters do not only depend on the width of the attached tip, but also on the mass and the intrinsic damping of the entire cantilever. Therefore, the parameter values do not necessarily decrease with the tip width, as shown by the location of the tip D marker in the c_3-c_4 plane (Figure 9). The PZT bending actuator, with tip D has being attached, was not sealed by a protective coating, and thus features a lower intrinsic damping. However, the parameter fitting process described above yields parameter values considering such different behaviors of the cantilevers.

For a validation of the model, the parameters determined above were used to calculate the values of ω_1 and T_1 for each tip-liquid combination. These calculated values are indicated by crosses (+) in Figure 7 and are in good agreement with the experimental data.

At last, we use the model parameters obtained above to determine the viscosity and density of an olive oil sample. The measurement results, that is, the resonance frequencies ω_1 and the time constants T_1 of the cantilevers immersed in the sample liquid are given in Table 3. From these results, the density and the viscosity of the liquid are calculated using (19), respectively.

5. CONCLUSION

The change of the dynamic behavior of a vibrating cantilever allows to investigate the physical properties of liquids. Various types of small tips of different geometries are attached to the cantilever and immersed into the sample solutions. The liquid surrounding the cantilever tip changes both the resonance frequency and the damping of the entire cantilever structure. To be able to conclude, from the measured frequency response to the liquid's parameters, an analytical model is needed. The developed model is based on the forces acting on an oscillating sphere in liquid, but generalized model parameters are used to consider the actual geometries of the applied cantilever tips. These parameters, furthermore, include the electrical and mechanical characteristics of the beam, which, therefore, must not be known. The model proved to be well suited for the characterization of various cantilevers and tip geometries by measuring in liquids with known density and viscosity. To extract the model parameters from the measured data, a curve fitting procedure was performed. The obtained parameters are specific for each cantilever tip and allow the subsequent simultaneous determination of density and viscosity of unknown liquids. Compared to other works, the sensor features high-quality factors of the considered resonance mode even for highly viscous liquids, greatly extending the measurement range.

ACKNOWLEDGMENTS

The authors would like to thank the Institute for Measurement Technology of the Johannes Kepler University (JKU), Linz, Austria, for providing the laser vibrometer used, and Professor Hans Irschik and Dr. Manfred Nader of the Institute of Technical Mechanics (JKU Linz), and Roman Beigelbeck of the Research Unit for Integrated Sensor Systems, Austrian Academy of Sciences, for useful discussions on the beam theory. This work was supported by the Austrian Science Fund (FWF) Project L103-N07.

REFERENCES

[1] E. Nwankwo and C. J. Durning, "Fluid property investigation by impedance characterization of quartz crystal resonators—part I: methodology, crystal screening, and Newtonian fluids," *Sensors and Actuators A*, vol. 72, no. 2, pp. 99–109, 1999.

[2] E. Nwankwo and C. J. Durning, "Fluid property investigation by impedance characterization of quartz crystal resonators—part 2: parasitic effects, viscoelastic fluids," *Sensors and Actuators A*, vol. 72, no. 3, pp. 195–202, 1999.

[3] B. Jakoby and M. J. Vellekoop, "Viscosity sensing using a Love-wave device," *Sensors and Actuators A*, vol. 68, no. 1–3, pp. 275–281, 1998.

[4] B. Jakoby, M. Scherer, M. Buskies, and H. Eisenschmid, "An automotive engine oil viscosity sensor," *IEEE Sensors Journal*, vol. 3, no. 5, pp. 562–568, 2003.

[5] B. Jakoby and M. J. Vellekoop, "Physical sensors for water-in-oil emulsions," *Sensors and Actuators A*, vol. 110, no. 1–3, pp. 28–32, 2004.

[6] A. Agoston, F. Keplinger, and B. Jakoby, "Evaluation of a vibrating micromachined cantilever sensor for measuring the viscosity of complex organic liquids," *Sensors and Actuators A*, vol. 123-124, pp. 82–86, 2005.

[7] P. I. Oden, G. Y. Chen, R. A. Steele, R. J. Warmack, and T. Thundat, "Viscous drag measurements utilizing microfabricated cantilevers," *Applied Physics Letters*, vol. 68, no. 26, pp. 3814–3816, 1996.

[8] J. W. M. Chon, P. Mulvaney, and J. E. Sader, "Experimental validation of theoretical models for the frequency response of atomic force microscope cantilever beams immersed in fluids," *Journal of Applied Physics*, vol. 87, no. 8, pp. 3978–3988, 2000.

[9] C. Bergaud and L. Nicu, "Viscosity measurements based on experimental investigations of composite cantilever beam eigenfrequencies in viscous media," *Review of Scientific Instruments*, vol. 71, no. 6, pp. 2487–2491, 2000.

[10] S. Boskovic, J. W. M. Chon, P. Mulvaney, and J. E. Sader, "Rheological measurements using microcantilevers," *Journal of Rheology*, vol. 46, no. 4, pp. 891–899, 2002.

[11] A. R. H. Goodwin, A. D. Fitt, K. A. Ronaldson, and W. A. Wakeham, "A vibrating plate fabricated by the methods of microelectromechanical systems (MEMS) for the simultaneous measurement of density and viscosity: results for argon at temperatures between 323 and 423 K at pressures up to 68 MPa," *International Journal of Thermophysics*, vol. 27, no. 6, pp. 1650–1676, 2006.

[12] C. Riesch, A. Jachimowicz, F. Keplinger, E. K. Reichel, and B. Jakoby, "A novel sensor system for liquid properties based on a micromachined beam and a low-cost optical readout," in *Proceedings of the 6th IEEE Conference on Sensors (ICSENS '07)*, pp. 872–875, Atlanta, Ga, USA, October 2007.

[13] I. Etchart, H. Chen, P. Dryden, et al., "MEMS sensors for density-viscosity sensing in a low-flow microfluidic environment," *Sensors and Actuators A*, vol. 141, no. 2, pp. 266–275, 2008.

[14] W. Y. Shih, X. Li, H. Gu, W.-H. Shih, and I. A. Aksay, "Simultaneous liquid viscosity and density determination with piezoelectric unimorph cantilevers," *Journal of Applied Physics*, vol. 89, no. 2, pp. 1497–1505, 2001.

[15] T. L. Wilson, G. A. Campbell, and R. Mutharasan, "Viscosity and density values from excitation level response of piezoelectric-excited cantilever sensors," *Sensors and Actuators A*, vol. 138, no. 1, pp. 44–51, 2007.

[16] B. Weiss, E. K. Reichel, and B. Jakoby, "Modeling of a clamped-clamped beam vibrating in a fluid for viscosity and density sensing regarding compressibility," *Sensors and Actuators A*, vol. 143, no. 2, pp. 293–301, 2008.

[17] J. E. Sader, "Frequency response of cantilever beams immersed in viscous fluids with applications to the atomic force microscope," *Journal of Applied Physics*, vol. 84, no. 1, pp. 64–76, 1998.

[18] C. A. Van Eysden and J. E. Sader, "Small amplitude oscillations of a flexible thin blade in a viscous fluid: exact analytical solution," *Physics of Fluids*, vol. 18, no. 12, Article ID 123102, 11 pages, 2006.

[19] C. Atkinson and M. Manrique de Lara, "The frequency response of a rectangular cantilever plate vibrating in a viscous fluid," *Journal of Sound and Vibration*, vol. 300, no. 1-2, pp. 352–367, 2007.

[20] "Argillon data sheet for bending actuators," Argillon GmbH, Redwitz, Germany, 2003, http://www.argillon.com.

[21] H. Parkus, *Mechanik der festen Körper*, Springer, Wien, Austria, 1960.

[22] M. Nader, *Compensation of vibrations in smart structures: shape control, experimental realization and feedback control*, Ph.D. dissertation, Johannes Kepler University, Linz, Austria, 2007.

[23] L. D. Landau and E. M. Lifshitz, *Fluid Mechanics*, Pergamon Press, London, UK, 1959.

Special Issue on Radio Frequency Integrated Circuits (RFICs)

Call for Papers

Radio Frequency Integrated Circuits (RFICs) are the most important building block in today's burgeoning personal communication and mobile multimedia devices. Innovation in the design and fabrication of RFIC components is thus vital for the fast growing wireless communication-based electronic devices for consumer and business applications. RFIC components include complete RF transceivers, as well as smaller building blocks such as low noise amplifiers (LNAs), local oscillators (LOs), frequency synthesizers, power amplifiers, and bandpass intermediate-frequency filters. Although CMOS is the prevalent process technology for analog-integrated circuit design, RFIC design is being explored in quite a few other process technologies such as standard bipolar technology, Si-Ge hetero-junction bipolar technology, GaAs technology, as well as other ternary semiconductor technologies such as $AlGa_xAs_{x-1}$. Therefore, some investigations into RFIC design using technologies other than CMOS, as we reach physical speed limitations in deep nanometer CMOS, are also very important. Next, the RF circuit design techniques for different frequency bands ranging from hundreds of MHz to millimeter wave lengths (~60 GHz) encompassing various RF and microwave communication standards is of interest to the RFIC design research and product development community. In addition, the currently emerging nanometric CMOS process technologies at 65 nm node and below using high-K dielectric also provide exciting opportunity for novelty in millimeter wave-length RFIC design. Computer-aided design tools, simulation platforms, and mathematical modeling for RFIC design are also a crucial aspect of designing RF circuits to specifications to end applications and communication standards. Hence, the aim of this special issue is to provide a unified framework to witness the progress of RF circuit design techniques in the context of the varying process technology and technology scaling platforms as well as the wide-range frequency bands and communication standards. This special issue solicits original research papers in the following areas and related areas without restrictions:

- RF circuit design techniques
- CMOS RFIC design techniques
- RFIC design using compound semiconductor process technologies
- Si-Ge HBT RFIC design techniques
- Millimeter wave-length integrated circuit design
- Intermediate frequency bandpass filters
- LNAs, RF oscillators, and frequency synthesizers
- RF circuit design for bluetooth, UWB, multistandard, ISM, GSM, RFID, software radio, and so on
- Modeling and computer-aided design techniques for RFIC design

Before submission authors should carefully read over the journal's Author Guidelines, which are located at http://www.hindawi.com/journals/apec/guidelines.html. Prospective authors should submit an electronic copy of their complete manuscript through the journal Manuscript Tracking System at http://mts.hindawi.com/ according to the following timetable:

Manuscript Due	March 1, 2010
First Round of Reviews	June 1, 2010
Publication Date	September 1, 2010

Lead Guest Editor

Rezaul Hasan, Center for Research in Analog and VLSI Microsystems Design (CRAVE), School of Engineering and Advanced Technology (SEAT), Massey University, Albany, Auckland 0632, New Zealand; hasanmic@massey.ac.nz

Guest Editor

Manh Anh Do, Center for Integrated Circuits and Systems, School of Electrical and Electronic Engineering, Nanyang Technological University, 50 Nanyang Avenue, Singapore 639798; emado@ntu.edu.sg